Available online at www.sciencedirect.com

SciVerse ScienceDirect

Acta Materialia 60 (2012) 1038–1047

Acta MATERIALIA

www.elsevier.com/locate/actamat

Observations of grain boundary impurities in nanocrystalline Al and their influence on microstructural stability and mechanical behaviour

F. Tang [a], D.S. Gianola [b], M.P. Moody [a], K.J. Hemker [c], J.M. Cairney [a,*]

[a] Australian Centre for Microscopy and Microanalysis, University of Sydney, NSW 2006, Australia
[b] Materials Science and Engineering, University of Pennsylvania, Philadelphia, PA 19104, USA
[c] Mechanical Engineering, Johns Hopkins University, Baltimore, MD 21218-2682, USA

Received 11 August 2011; received in revised form 31 October 2011; accepted 31 October 2011

Abstract

The exceptional properties of nanocrystalline materials lend themselves to a wide range of structural and functional applications. There is recent evidence to suggest that grain boundary impurities may have a dramatic effect on the stability, strength and ductility of nanocrystalline metals and alloys. In this study, transmission electron microscopy and atom probe tomography were used to characterize specimens deposited at different base pressures, thus providing a direct comparison of impurity content with microstructural stability and mechanical behaviour. Atom probe measurements provide clear experimental evidence of grain boundary segregation of oxygen in samples deposited at higher base pressures. It is proposed that these oxygen atoms pin the boundaries, preventing stress-assisted grain growth and resulting in increased strength and loss in ductility. This study provides the first direct experimental evidence that boundary impurities play a critical role in determining the microstructural stability and deformation behaviour of nanocrystalline metals.

Keywords: Nanocrystalline; Impurity segregation; Deformation; Aluminium; Atom probe tomography

1. Introduction

Nanocrystalline and nanostructured materials offer properties that are vastly different from and often superior to those of conventional microcrystalline materials. Improvements include, but are not limited to, higher strength, enhanced hardness [1], greater diffusivity and self-healing of radiation-induced damage through the absorption and recombination of point defects [2]. Processing difficulties have inhibited their use as bulk structural materials, but nanocrystalline thin films, membranes, laminates and coatings are becoming very common in micro- and nanoscale structures and devices.

The unique properties of nanocrystalline materials are directly related to the ubiquitous presence of grain boundaries. These grain boundaries are often thought of as static obstacles to dislocation or magnetic boundary motion, pathways for atomic and thermal transport, and sinks and sources of point defects and dislocations. Their existence and stability are crucial to the long-term performance of nanocrystalline devices, but they are not nearly as static as is generally assumed. Nanocrystalline materials are inherently metastable, since thermally or mechanically driven grain growth leads to a reduction in overall grain boundary content and energy. In some instances abnormal grain growth has been associated with exposure to elevated temperatures, but many experimental observations suggest that thermally assisted grain growth in nanocrystalline materials is modest at intermediate temperatures [2,3]. This unexpected thermal stability has been attributed to a

* Corresponding author. Tel.: +61 2 9351 4523; fax: +61 2 9351 7682.
E-mail address: julie.cairney@sydney.edu.au (J.M. Cairney).

1359-6454/$36.00 © 2011 Acta Materialia Inc. Published by Elsevier Ltd. All rights reserved.
doi:10.1016/j.actamat.2011.10.061

number of hypothetical factors, including solute and pore drag, chemical ordering and geometric frustration. By contrast, the mechanical stability of nanocrystalline materials has been shown to be much lower than originally expected. Mechanically induced room temperature grain growth in nanocrystalline metals has been associated with indentation [4–6], compression loading [7,8], tensile loading [9–12] and mechanical fatigue [13]. Experiments quantifying the growth in terms of temperature [6], strain rate [12], proximity to crack tips [14] and testing mode [7] also point to applied stress as the driving force for grain growth.

A recent study by Gianola and coworkers [15] supports the hypothesis that small amounts of impurities can have a dramatic effect on the strength and ductility of nanocrystalline metals. Micro-tensile testing of nanocrystalline Al (nc-Al) films revealed that the deposition base pressure, and presumably the attendant impurity concentration, have a dramatic influence on the mechanical behaviour. As shown in Fig. 1, samples deposited at higher base pressures (10^{-5} torr) showed a stable microstructure and a strong-but-brittle response, while those deposited at lower base pressures (10^{-7} torr) showed remarkable thermal stability, but a very different deformation response, namely moderate strength and over 15% strain to failure. Grain growth was only observed in the films deposited at lower base pressures. Stress-coupled grain growth is therefore thought to be affected by impurities at the grain boundaries, where a critical O impurity concentration appears to be required to pin or immobilize grain boundaries against the coupling of applied stress [15]. Recent molecular dynamics (MD) simulations of an Al tilt grain boundary decorated with O atoms [16] also support the notion of a changing critical stress required for coupled grain boundary motion due to an impurity pinning atmosphere.

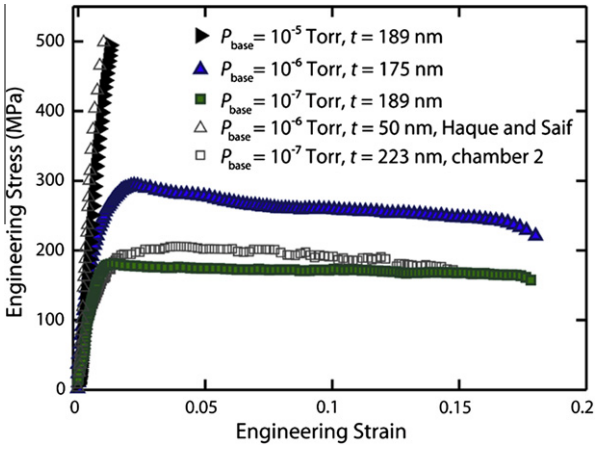

Fig. 1. RT tensile stress–strain curves for three batches of Al films, showing two distinct classes of mechanical behaviour. The transition from strong and ductile to stronger but brittle occurs at base pressures between 10^{-6} and 10^{-5} torr. For comparison, the stress–strain curves with open symbols represent the behaviour of nc-Al thin films deposited in other sputtering chambers, including a stress–strain curve for a similar nc-Al film deposited at relatively high base pressure [54].

Recent studies also suggest that impurities, in addition to affecting deformation behaviour, play a large role in the thermal stability of nanocrystalline microstructures, a critical issue in the development of commercial materials. For grains on the micron length-scale, the driving force for recrystallization (according to the Gibbs–Thompson equation), and therefore the recrystallization rate, is known to increase with decreasing grain size. However, studies have revealed that many nanocrystalline materials exhibit much better stability than predicted. For example, pure nc-Al prepared by mechanical attrition revealed grain size stability up to temperatures as high as $0.78T_m$ [17]. This stability has been attributed to the effect of solute atoms at the grain boundaries, either by impurity drag associated with grain growth [17,18] or by creating a state of metastable thermodynamic equilibrium which eliminates the driving force for grain coarsening [19].

Despite this evidence to suggest the importance of grain boundary impurities for both deformation and stability, a complete understanding of the role of trace-level impurities has been hindered by the technical difficulties involved with direct experimental measurements of grain boundary segregation. There are inherent challenges in the high-resolution microstructural analysis of nanocrystalline materials. Auger and secondary ion mass spectroscopy techniques require a fractured surface or, where mapping is possible, are limited by their low in-plane spatial resolution. Transmission electron microscopy (TEM) can provide information about the grain size and morphology. However, overlapping of grains in the thin foil precludes direct examination of the boundaries between the grains, and chemical analysis of small concentrations of impurities using electron energy loss spectroscopy is typically limited by the resolution of the instrument. Alternatively, atom probe tomography (APT) provides three-dimensional maps showing the elemental distribution at the atomic scale and may be used to characterize the segregation of elemental species to the grain boundary [20]. Light elements can be easily distinguished, and the detection limit is on the order of single atoms. It is therefore highly suited to the study of low-level grain boundary segregation. Unlike beam-based techniques, APT provides a means to directly determine interfacial segregation in three dimensions.

In the current study, both TEM and APT have been used to characterize the microstructure and segregation in samples that have been deposited at different base pressures. The samples investigated were the same as those used in the study of Gianola et al. [15], which allows for direct comparison of impurity levels with mechanical behaviour.

2. Experimental

For this study, three nc-Al films were prepared using magnetron sputtering at three different base pressures (to introduce different levels of impurities). The films were deposited on Si wafers by pulsed DC magnetron sputtering of a 99.999% pure Al target at base pressures of $\sim 1 \times 10^{-7}$,

$\sim 2 \times 10^{-6}$ and $\sim 1 \times 10^{-5}$ torr to a nominal thickness of 180 nm (for the sake of brevity, the sample deposited at $\sim 2 \times 10^{-6}$ is referred to from here on by the order of magnitude, i.e., as the sample deposited at 10^{-6} torr). Micro-tensile testing was carried out with a custom-built micro-sample tensile testing apparatus (described in detail in Refs. [21,22]) at a constant strain rate of $4 \times 10^{-5}\ s^{-1}$. Strain was measured locally in the gauge section of the sample using a custom digital image tracking system, with fine silica powder used as markers for tracking [22,23].

TEM was carried out on freestanding films in plan view with a JEOL 3000F in bright field and selected area diffraction mode. Site-specific atom probe specimens were prepared in a FEI Helios NanoLab 600 Dual Beam focused ion beam (FIB)/scanning electron microscope using a "lift-out" method [24,25] whereby micron-sized pieces of the specimen are cut and lifted out and welded to a prefabricated Si array. Before preparation, a layer of Ni was sputter coated onto the surface to protect the top edge. A combination of scanning electron microscopy imaging and energy dispersive spectroscopy was used to monitor the tip during milling to ensure that the Al film remained, and low accelerating voltages (2 keV) were used in the final stages to minimize Ga implantation. Atom probe experiments were conducted with an Imago Scientific (now Cameca) LEAP® 3000X Si instrument. Several data sets were collected from each sample. For the sample deposited at the lowest base pressure, voltage mode was used with a base temperature of 40 K, while the other two samples were analysed in laser mode with a laser energy of 0.5 nJ at 20 K (to improve the rate of running the samples successfully). Three-dimensional (3D) reconstruction and visualization were performed using the commercial IVAS™ software. Crystallographic poles observed in field desorption maps and TEM images of the tips were used to calculate and set reconstruction parameters [26]. An initial analysis of the data displayed significant O peaks, and O segregation was noted in at least one of the samples. No obvious segregation of any other element was noted at the grain boundaries. Therefore, efforts were focused primarily on accurate measurement of the concentration and distribution of O atoms. Visualization of O was undertaken using the O^+ peak at a mass-to-charge ratio of 16. The measurement of O content and concentration profiles was conducted using the O^+ peak as well as the portion of the smaller O_2^+, AlO^+, AlO^{2+} and Al_2O^{3+} peaks (where present) that can be attributed to O. Gibbsian interfacial excess values were calculated from cumulative diagrams (sometimes referred to as the "ladder method"; see for example Ref. [27]) using a custom MATLAB (Mathworks Inc.) script.

3. Results

3.1. TEM

TEM images (Fig. 2) show a variation in the grain size with the different deposition parameters. Higher base pressures resulted in progressively smaller grain sizes, with the samples deposited at $\sim 10^{-7}$, 10^{-6} and 10^{-5} torr having average grain sizes of 36, 25 and 13 nm, respectively. Indexing of selected area diffraction patterns (shown as an inset in the micrographs in Fig. 2) revealed only reflections from the face centred cubic Al structure, with no evidence of any other crystalline phase. Previous high-resolution TEM studies [15] showed sharp interfaces, with no evidence of second-phase particles in the bulk or at the grain boundary.

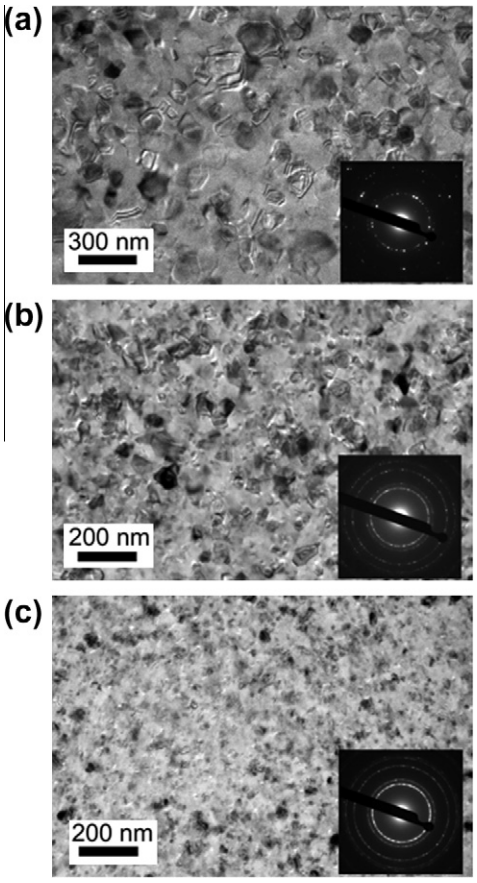

Fig. 2. Bright field TEM images of the samples deposited at (a) 1×10^{-7}, (b) 2×10^{-6} and (c) 1×10^{-5} torr. Diffraction patterns from each sample are inset.

3.2. APT

The compositions of the films deposited at 10^{-7}, 10^{-6} and 10^{-5} torr were measured using the atom probe, and the results indicated average oxygen contents of 0.05 ± 0.01, 0.18 ± 0.01 and 1.76 ± 0.05 at.%, respectively. The deposition base pressures, average grain sizes (measured by TEM), average compositions and the yield strengths of each set of films [15] are listed in Table 1. These results support the suggestion that mechanical behaviour is governed by low levels of oxygen impurities, although closer inspection is needed to confirm this hypothesis and determine the role that these impurities play.

Reconstructed atom probe images are shown in Fig. 3. These images are subsets of larger data sets which have

Table 1
The deposition base pressure, yield strength [16] approximate grain size (from TEM) and measured O-content (from atom probe) of the three samples.

Sample	Deposition base pressure (torr)	Yield strength (MPa)	Average grain size (nm)	Measured oxygen (at.%)
Low impurity	1×10^{-7}	129	36	0.05 ± 0.01
Med impurity	2×10^{-6}	222	25	0.18 ± 0.01
High impurity	1×10^{-5}	495	13	1.76 ± 0.05

been cropped to a volume of $50 \times 50 \times 5$ nm to show individual grains and grain boundaries. In these images, the O atoms are shown as large red spheres, and the Al atoms as small green dots. Ga atoms are also seen along the grain boundaries, represented by medium-sized blue spheres, and are an artefact of the FIB specimen preparation process due to the well-documented affinity of Ga for grain boundaries in Al [28–30]. The O atoms are clearly associated with the grain boundaries in the samples with the smallest grains (Fig. 3c), but it is not obvious from visual inspection whether there is any relationship between the grain boundaries and the location of the O atoms in the samples deposited at lower base pressures (Fig. 3a and b). A few of the atom probe data sets from the sample deposited at the highest base pressure (the highest O sample) also contained regions (up to a few nanometres in size) which are very rich in O at the triple points between grains.

Fig. 4a and b shows selected regions from the data sets obtained from the films deposited at the two higher base pressures (2×10^{-6} and 1×10^{-5} torr). Cylindrical volumes of data have been selected to measure the composition profile across the interfaces along the length of the cylinders. For each sample, two representative cylinders are displayed. Fig 5a shows the average measured composition across the interface for seven to ten selected volumes, where the concentration maxima have been aligned before averaging. No O was detected at the interface for the sample deposited at 1×10^{-7} torr (the low impurity sample) and, as a result, these data are not shown on the plot. Very little O was detected at the interface for the selected areas for the sample deposited at 2×10^{-6} torr (the medium impurity sample) so the compositional profile is quite flat. For the sample deposited at 1×10^{-5} torr, significant O can be discerned. However, in both the medium and high base pressure samples, the segregation profile varied dramatically from interface to interface, which is reflected in the large error bars given in these plots (the error shown is the standard deviation in the composition measurements at each point). This variation in the measured segregation has a number of possible causes. First, it is expected that grain boundary character (low angle/high angle/special boundaries) will affect the extent of segregation [31]. Secondly, it is well established that artefacts due to local magnification effects occur in atom probe data from interfaces and can lead to spreading of segregated species over a grain boundary compared to the actual composition profile. These effects vary considerably, depending on the orientation of the grain boundary with respect to the analysis direction, being maximum where the boundary is parallel to the analysis direction and minimum where the boundaries are perpendicular [32]. Therefore, the best way to measure the segregation to an interface from atom probe data is to report the number of segregating atoms per unit area, or the Gibbsian interfacial excess Γ. This value should not be affected by any lateral spreading of the atoms across the interface. For the selected cylindrical volumes across the interfaces, the average interfacial excess values were determined as 0, 0.23 and 1.31 atoms nm^{-2} for the samples deposited at 10^{-7}, 10^{-6} and 10^{-5} torr, respectively. The interfacial excess values are shown in Fig. 5b. The error is again the standard deviation of the interfacial

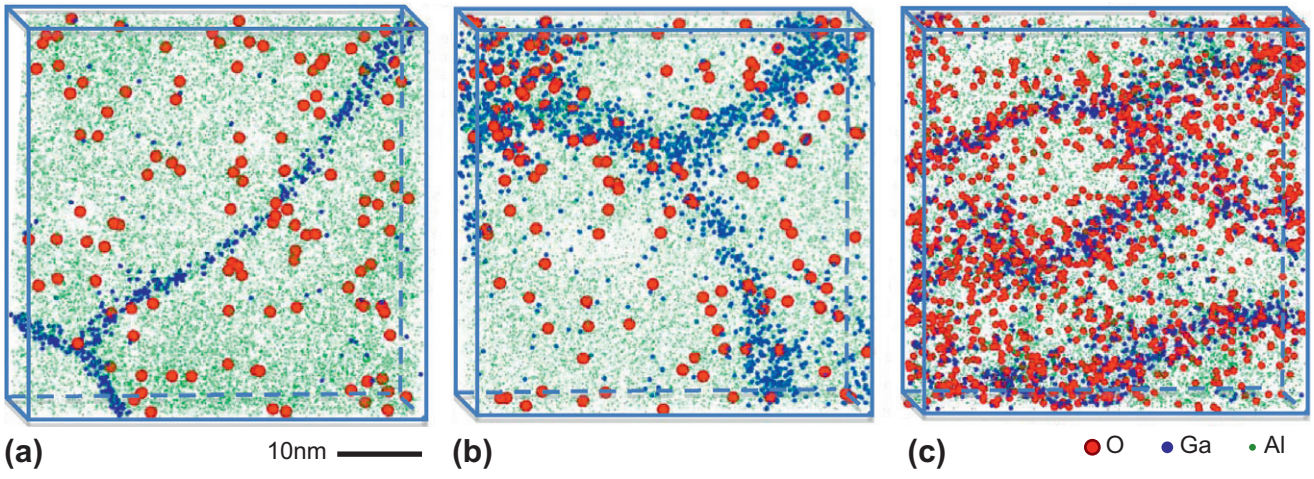

Fig. 3. Reconstructed atom probe images of the samples deposited at (i) 1×10^{-7}, (ii) 2×10^{-6} and (iii) 1×10^{-5} torr. The volume in each case is $50 \times 50 \times 5$ nm. The large red spheres represent O atoms, the smaller blue spheres represent Ga atoms and the light green dots represent the Al matrix atoms (for visual clarity, only 2% of the Al atoms are shown). (For interpretation of the references to colour in this figure legend, the reader is referred to the web version of this article.)

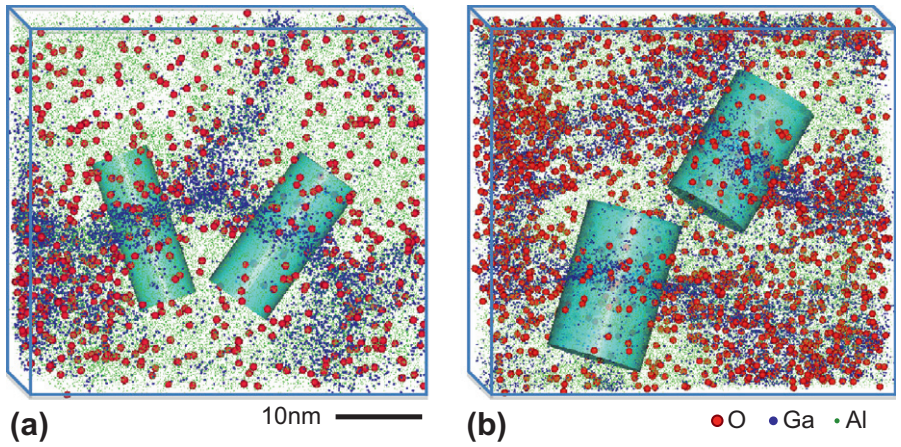

Fig. 4. Reconstructed atom probe images of the samples deposited at (a) 2×10^{-6} (medium pressure) and (b) 1×10^{-5} torr (the highest pressure). Here, typical cylindrical volumes selected for the determination of composition profiles across the interface are shown. The volume in each case is $50 \times 50 \times 10$ nm. The large red spheres represent O atoms, the smaller blue spheres represent Ga atoms and the light green dots represent the Al matrix atoms (for visual clarity, only 3% of the Al atoms are shown). (For interpretation of the references to colour in this figure legend, the reader is referred to the web version of this article.)

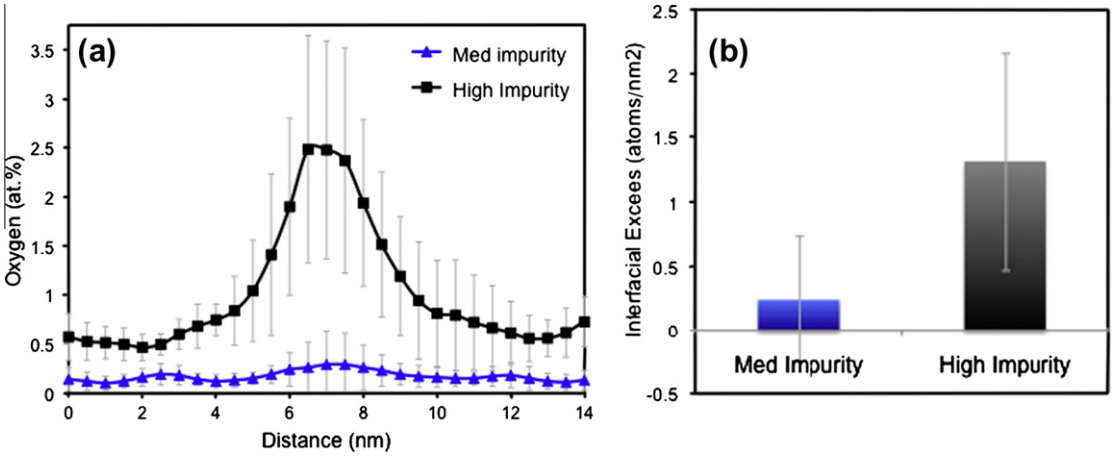

Fig. 5. (a) Average 1D composition profile through 7–10 cylindrical volumes taken through grain boundaries for the sample deposited at 2×10^{-6} torr (medium impurity level) and 1×10^{-5} torr (the highest impurity level). The error bars show the standard deviation, indicating the significant variability between the profiles observed. (b) Average Gibbsian interfacial excess at grain boundaries calculated from the same cylindrical volumes. The sample deposited at the lowest base pressure did not display any detectable O segregation and is not shown.

excess values measured, and it is clear that there is still a large variation in the extent of segregation observed between different interfaces.

The determination of the interfacial excess values from the cylindrical volumes of data still has limitations. First, it is limited by the manual selection of the regions in which to apply the cylinder, which could lead to a non-random choice of grain boundaries (i.e., it is possible that the boundaries with the most segregation or the longest and straightest boundaries are selected). In addition, it does not take into account segregation at and around the triple points in the data, which are deliberately avoided. Also, the volume of the area analysed is only limited to the selected areas, and the orientation of the cylinders perpendicular to the grain boundary is based on a visual assessment. For an improved analysis of the average composition of O relative to the position of the grain boundary regions, a proximity histogram (proxigram) analysis [33] was applied to the atom probe data.

A proxigram analysis is a method that can be used to compare the grain boundary composition in a 3D dataset. In this case, a Ga isoconcentration surface (2% Ga) is defined which neatly encapsulates the grain boundary areas. Fig. 6 shows both a reconstructed atom map from the low impurity sample in which the Ga atoms are displayed as blue spheres (Fig. 6a) and an image of the same volume in which a 2% Ga isoconcentration surface is shown (Fig. 6b). From this surface it is possible to calculate the average composition moving away from the surface both in towards the grain boundary and out into the grains, providing a concentration profile which accounts for the 3D nature of the grain boundaries. This result is

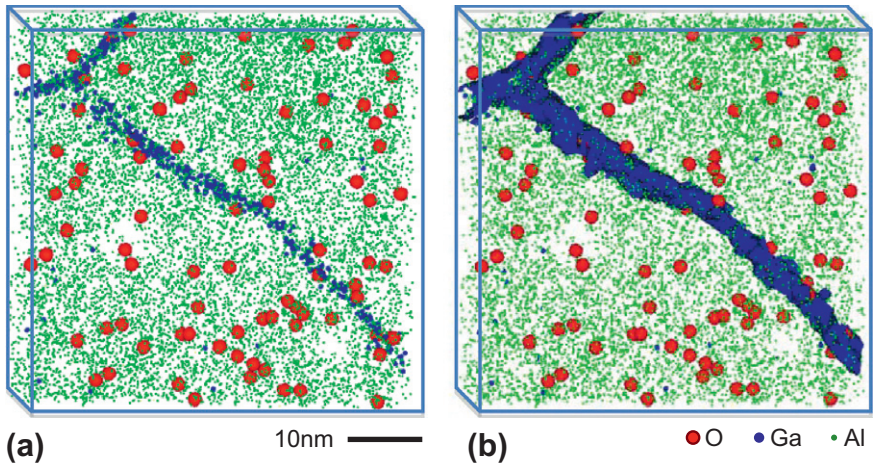

Fig. 6. Reconstructed atom probe images of the samples deposited at 1×10^{-7} torr (the lowest pressure/lowest impurity level). The volume in each case is $50 \times 50 \times 5$ nm: (a) shows a typical atom map, where the large red spheres represent O atoms, the smaller blue spheres represent Ga atoms and the light green dots represent the Al matrix atoms (3% shown), (b) shows a 2% Ga isoconcentration surface that encapsulates the grain boundary regions. (For interpretation of the references to colour in this figure legend, the reader is referred to the web version of this article.)

more informative than a simple set of one-dimensional concentration profiles though cylinders that pass through selected grain boundaries. It averages any effects from different levels of segregation to different boundaries as well as any effects that arise from trajectory aberrations in atom probe data when the boundaries are oriented differently with respect to the analysis direction.

Fig. 7 shows the resulting proxigram in which the O composition profile was determined at progressively greater distances normal to the grain boundary, as defined by the Ga surface. For the highest O concentration sample, two curves are presented: one for data that include O-rich regions observed at triple points, and one for data that do not. It is clear that the sample with the highest O concentration also displays the greatest amount of O segregation. Some segregation is also observed in the sample deposited at intermediate base pressures (medium O level) and the segregation in the most pure sample is minimal.

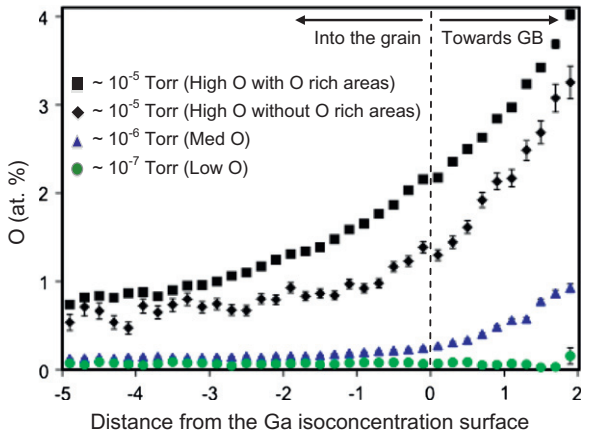

Fig. 7. A proximity histogram showing the measured O concentration about a Ga isoconcentration surface (a 1% Ga surface was used for the samples deposited at 1×10^{-7} and 2×10–6 torr and a 3% Ga surface was used for the samples deposited at 1×10^{-5} torr).

4. Discussion

The segregation profiles in Fig. 7 can be directly compared with the results of the micro-tensile tests on the same samples, shown in Fig. 1, which revealed a markedly different response for the three film batches. The samples deposited at the highest base pressure (highest O level) displayed dramatically enhanced strength over coarse-grained Al, but an even more dramatic loss of tensile ductility or elongation to failure. Lowering the base pressure (decreasing the impurities) led to a progressively lower strength and much higher elongation. Most striking is the sample deposited at the intermediate base pressure, which displays enhanced strength, together with good elongation. Comparisons with the mechanical response of nc-Al films deposited in other sputtering chambers (open symbols in Fig. 1 [34]) supports the observation that the base pressure during deposition plays a role in controlling strength and ductility.

However, in order to draw a conclusion about the relationship between the segregation and the observed mechanical properties in terms of microstructural stability, it is prudent first to examine the likely effect that the observed oxygen might have in terms of solid solution strengthening from dislocation–solute interactions.

4.1. Potency of solid solution strengthening

The negligible equilibrium solubility of O in Al suggests that the presence of supersaturated O solutes in these thin films is due to non-equilibrium effects such as those arising from the kinetics of the sputtering process. Given the relatively high concentration of solute measured by APT, the mean solute spacing may be smaller than the mean grain size and could lead to significant strengthening. Indeed, using the bulk concentration values c and calculating the mean spacing as $\lambda = b/(2c)^{1/2}$, where b is the Burgers

vector, $\lambda_{low} \approx 9$ nm ($d/\lambda \approx 7$) for the lowest base pressure films and $\lambda_{high} \approx 2$ nm ($d/\lambda \approx 7$) for the highest base pressure.

Assuming a classical dislocation interaction with a solute atmosphere, the stress required to glide a dislocation between two pinning points imposing a resistance force of f_{obs} can be expressed as $\tau = f_{obs}/b\lambda$. The component of strengthening that arises from the presence of solutes in a lattice is often expressed in the general form as

$$\tau_{SS} = \beta G \varepsilon^p c^q \quad (1)$$

where G is the shear modulus of the solvent, c is the concentration of solute, β is an empirically determined proportionality constant related to the obstacle strength, and ε is termed an interaction parameter. In the special case of substitutional solid solution strengthening in metals (valency differences between solute and solvent can be neglected to first order), wherein a spherical stress state reasonably describes the solute matrix mismatch, ε reduces to the misfit strain quantity $\varepsilon = |(r_{solvent} - r_{solute})/r_{solvent}|$, where $r_{solvent}$ and r_{solute} are the atomic radii of solvent and solute, respectively. The values of the exponents p and q in Eq. (1) depend on the nature of the model describing the statistical average of the solute spacing and the dislocation–solute interaction strength. Of the many available models for solid solution strengthening, here the case of the well-known Fleischer model is considered as applied to dilute substitutional solutes in a cubic metal solvent [35], in which ε encapsulates changes to the lattice parameter and shear modulus (both affecting dislocation motion through the lattice) and scales as $p = 3/2$, while concentration scales with $q = 1/2$. The Labusch theory [36] is also considered, which gives $p = 4/3$ and $q = 2/3$, and assumes more concentrated solutions with strong localized interactions.

The increase in yield strength for the nc-Al films with different impurity concentrations as a function of O concentration is plotted in Fig. 8. The observed change in yield strength is shown in comparison with both the O concentration of the grain interiors (which is the value that would be expected to contribute to classical solid solution strengthening), as well as in comparison with the overall amount of O present (as an upper bound for the number of O atoms that could contribute to strengthening). These measured values are compared with the predictions offered by the Fleischer and Labusch models for $\beta = 0.01$ and 0.1 (which represent a range of both soft substitutional and harder solute obstacles, owing to the possibility of tetragonal strain fields arising from interstitial solutes [37]).

For these predictions of solid solution strengthening, it is clear that the presence of solute alone cannot account for the large increase in yield strength that was measured in the Al–O films, which suggests that the microstructural stability of the films under stress plays a dominant role in strengthening. It is noted that the effects of grain size and distribution, which vary with impurity concentration, are expected to play an additive role in strengthening [38]. To reconcile the measured mechanical response properly, the dynamic nature of stress-driven microstructural evolution needs to be considered: namely, immobile grain boundaries during plastic deformation in the case of the highest O content appear to be potent strengtheners, albeit with limited ability to sustain large plastic strains, as discussed in detail in Refs. [11,15]. In contrast, the films with low and intermediate impurity contents demonstrated copious microstructural evolution during deformation, intermediate strength values and relatively large tensile ductility. These observations and analyses imply a critical concentration of O at the grain boundary to sufficiently hinder motion under applied stresses. Attention now turns to microstructural stability, and segregation measurements from the atom probe data sets are compared.

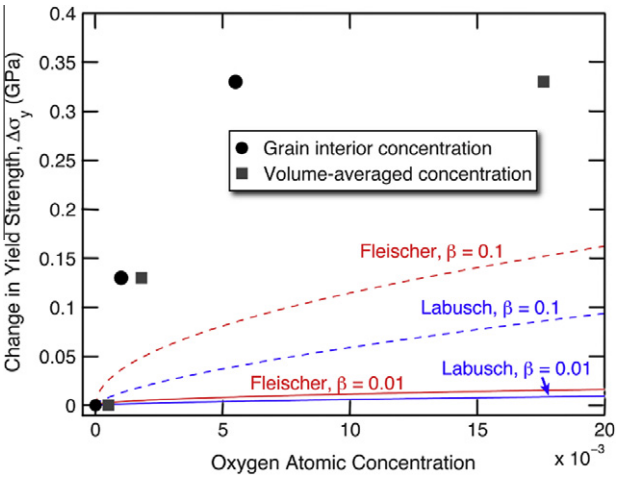

Fig. 8. Yield strength increase measured in nc-Al thin films as a function of the O concentration obtained from atom probe tomography analysis (both the grain interior concentration and the volume-averaged concentration are shown). The solid and dashed lines show predictions of the Fleischer and Labusch models for $\beta = 0.01$ and 0.1, respectively.

4.2. Stability of nanostructure due to the presence of solute and critical stress for coupled grain boundary migration

The results from the atom probe proxigram analysis of all Al–O films show a clear tendency for O to segregate to grain boundaries, given a sufficiently high concentration of O. The films deposited at the lowest base pressure do not show any segregation above the detection limit, while the intermediate and high base pressure films show the preference of the O to sit at grain boundaries (Fig. 7). Given that the intermediate impurity content films show stress-driven grain growth despite the propensity for segregation of O, while the high impurity content films remain microstructurally static, it is interesting to consider the minimum O content required to stabilize the microstructure.

Preferential segregation of O to grain boundaries in Al is due to the near-zero solubility in the grain interior and the abundance of spacious sites for the solute (relative to the lattice) with a lower potential energy for the mismatched solute. The presence of solute in the grain boundary serves

to decrease the grain boundary energy γ, as described by Gibb's adsorption equation [39]:

$$d\gamma = -\Gamma d\mu_{\text{solute}} \tag{2}$$

where μ_{solute} is the chemical potential of the solute. Following several researchers [40–44], Eq. (2) can be rewritten in the dilute limit in terms of the interfacial excess, the solute concentration and the enthalpy of segregation, ΔH_{seg}, as:

$$\gamma = \gamma_{\text{o}} - \Gamma(RT\ln c + \Delta H_{\text{seg}}) \tag{3}$$

where γ_{o} is the grain boundary energy of the pure solvent, R is the ideal gas constant, and T is the temperature. The thermodynamic implication from Eq. (3) is that a metastable equilibrium can exist, given sufficiently large Γ or ΔH_{seg} such as to give $\gamma \leqslant 0$, which can be considered in the context of a driving force due to excess free energy of grain boundaries with area A, given as $\int \gamma dA$. This framework also supports conventional wisdom that the driving force for grain growth increases with decreasing grain size (from the increase in A) [43,45], provided that a concomitant decrease in γ does not occur. Setting $\gamma = 0$ in Eq. (3) and rearranging, one can solve for a critical interfacial excess value required for microstructural stability:

$$\Gamma_{\text{cr}} = \gamma_{\text{o}}(RT\ln c + \Delta H_{\text{seg}})^{-1} \tag{4}$$

The microstructural stability of thepurest Al films with the lowest concentration of O and extent of grain boundary segregation was verified via TEM examination after dry storage at room temperature for 3 months (for Al, this corresponds to $0.32T_{\text{melt}}$). Indeed, the films retain their nanocrystalline grain sizes after these time intervals. Furthermore, the microstructure was found to be thermally stable with mild heating of the films, as demonstrated in Fig. 9, where grain size distributions for specimens in the as-deposited condition, and after heating at ~100 °C ($0.32T_{\text{melt}}$) for 15 min, are shown. No apparent grain growth was observed in the heated specimens, and the shape of the distribution can still be approximately described by a lognormal probability function. It is a reasonable extension to predict that the Al films with higher O content would similarly exhibit microstructural stability under similar thermal driving forces.

These observations point to the importance of the distinction between thermal driving forces for grain growth and those that arise directly from local shear stresses at grain boundaries which serve to promote coupled boundary migration, as identified by MD simulations [46] and experiments [10,47]. This notion is further supported by the observations of Zhang et al. [6], which show grain growth occurring during athermal indentation of nc-Cu at cryogenic temperatures. Here it is suggested that the pinning of grain boundaries by solutes endows the material with microstructural thermal stability, while applied stresses can promote depinning and coupled boundary migration, given a sufficiently high shear stress driving force [47]. However, the critical stress required for coupled grain boundary motion will be altered by the presence of segregated solute at the boundary as well as solute in the lattice in the path of a moving boundary. If resolved shear stresses along boundaries due to applied loads reach the critical value for coupled grain boundary motion, plastic strain can be accommodated directly via this grain growth mechanism. The addition of solute at grain boundaries will increase the critical stress for motion, akin to a dislocation depinning from a Cottrell atmosphere [37], and other deformation mechanisms that are typically associated with nanocrystalline metals with static microstructures will be activated prior to the occurrence of boundary motion [48] (such as partial dislocation nucleation [49], grain boundary sliding [50] or deformation twinning [51]). In other words, deformation mechanisms prevalent in static nanocrystalline microstructures compete with dynamic coupled boundary migration to relax the large stresses experienced in these materials. The critical stress at which one mechanism mode is favoured is biased by the presence of solute. This schematic view qualitatively supports the general observation by several researchers [7,52] that electrodeposited nc-Ni, which is known to possess impurities from the deposition bath, possesses surprising thermal stability and is not generally prone to stress-driven grain growth.

Elsener and colleagues [16] investigated a scenario where an Al bicrystal containing a symmetric tilt grain boundary was loaded in shear applied parallel to the boundary via MD simulations at 0 and 100 K. These authors introduced substitutional O solutes into the Al solvent by developing a variable charge transfer framework which is necessary to fully describe the metal–oxide interaction. These systems were studied under shear to simulate the interaction of a

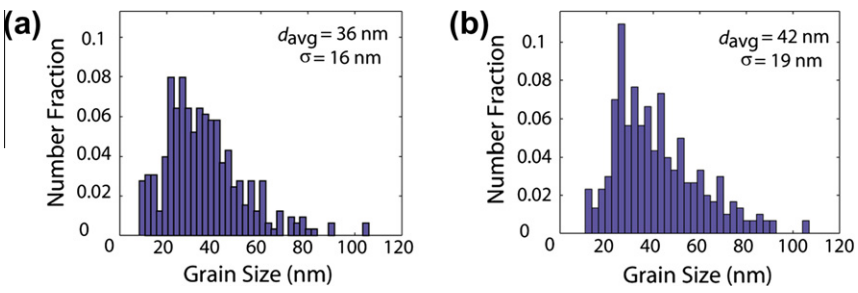

Fig. 9. Grain size distributions for a nc-Al thin film deposited at a base pressure of 10^{-7} torr (a) in the as-deposited condition and (b) after heating at 100 °C for 15 min.

grain boundary experiencing coupled motion with periodic arrays of solute atoms, and the resulting change in mechanical response, as a function of O concentration. An increase in the critical stress required for coupled migration was measured as a direct result of the altered stress fields surrounding the solute atoms in the presence of a moving interface. They found that, in a dilute solution where O–O interactions were negligible, the increase in stress required for coupled grain boundary migration was a linear function of the number of oxygen atoms, which they attributed to the additive effect of the local stress signature of each O atom during collective boundary motion. The MD results giving the magnitude of the critical shear stress increase upon addition of varied O solute planar density can be compared with the present experiments by approximating the planar array of O solutes in the MD simulations as an interfacial excess quantity. This is a reasonable estimation, to first order, since MD results for all O concentrations show the peak stress required for coupled motion to occur at the instant when the grain boundary plane is coincident with the planar solute array [16]. Thus, this critical stress value can be considered as the depinning event necessary to mobilize the boundary.

Fig. 10 shows the experimentally determined interfacial excess values for the three Al–O films and the yield strengths measured from tensile testing, compared with the results of the MD bicrystal simulations [16]. The MD results for critical shear stress required for coupled grain boundary motion at 0 and 100 K are shown as a function of planar excess from O solutes, along with the experimentally measured yield strength in shear, computed using a Taylor factor of 3.06 for a randomly oriented polycrystal [53]. A similar general trend in strengthening from increasing solute concentration is evident, despite the differences in geometry, strain rate and temperature, which render a comparison of absolute values difficult. One notable feature of the experiments is that the measured strengthening appears to deviate from the linear behaviour suggested by

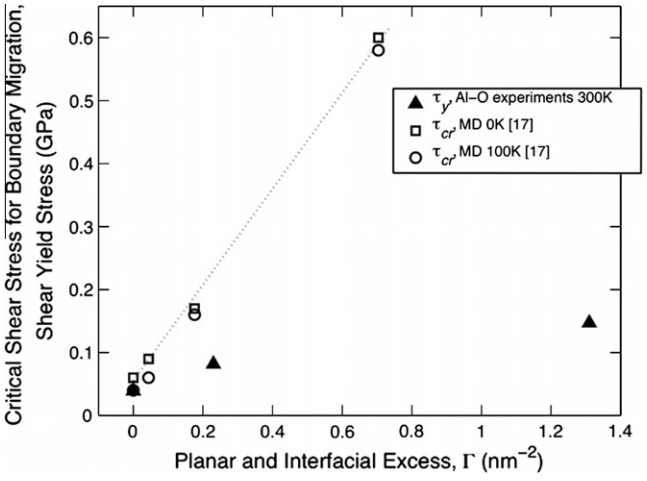

Fig. 10. Comparison of the critical shear stress required for coupled grain boundary migration (MD simulations, open symbols) [17] with experimentally measured yield strengths of Al–O thin films (closed symbols).

MD simulations, with increases in strength diminishing with increasing solute content. Despite its high strength, the highest O sample exhibits very limited ductility. Previous studies [48] indicate that nanocrystalline metals become much stronger with attendant reductions in tensile ductility when ordinary dislocation activity is mitigated. Stress-assisted room temperature grain boundary migration has been shown to dramatically increase the tensile ductility of nc-Al, albeit at slightly reduced overall strengths [11]. Stress-assisted boundary migration is itself a deformation mechanism, and boundary migration triggers stress-assisted grain growth which also allows increased dislocation plasticity.

Furthermore, in addition to the O segregation, it is possible that the O-rich regions observed at the triple points in some data sets contribute to the strength and elongation. A more systematic experimental study is the focus of ongoing research. Nevertheless, the observation that stress-driven grain growth only occurred in the low and medium O content films, while the high O content remained microstructurally stable throughout the plastic deformation process, places the critical interfacial excess for stress-driven stability between $\Gamma \approx 0.25\ \mathrm{nm}^{-2}$ and $\Gamma \approx 1.3\ \mathrm{nm}^{-2}$. The results are suggestive of a competition between alternate deformation mechanisms, based on the extent of solute segregation.

The ability to augment deformation mechanisms to accommodate stress via dynamic evolution and to control the threshold stress for grain boundary migration by local spatially controlled doping potentially allows for the tailoring of mechanical properties to specific applications, where the pinning of grain boundaries by impurities increases the stress required for stress-coupled grain growth and therefore allow higher strengths to be achieved for low grain size materials in the case where deformation is governed by stress-driven grain growth. Impurities at the grain boundaries may therefore offer the ability to provide enhanced strengths as the grain size is reduced, beyond those obtained for pure metals. It will of course be necessary to consider ductility and ultimately damage tolerance, which may be lost at very high impurity levels. It is necessary that doping is carefully controlled to achieve an optimum combination of strength and ductility, depending on the application.

There is now increasing evidence to suggest that very small levels of impurities play a much greater role in the deformation of nanocrystalline alloys than previously appreciated. The increase in strength observed when thin films are deposited at higher base-pressures (together with the absence of any second phases) [15,54] and the unusual grain size stability that is imparted by these modest levels of impurities [3,17] have already been mentioned. The minimum achievable grain size in nanocrystalline materials prepared by severe plastic deformation has been reported to be much higher in the case of pure metals than it is for alloys [55]. Moreover, it has been demonstrated that W-doped electrodeposited Ni can have a mean grain size <5 nm, which is considerably smaller than grain sizes that are typically achievable in pure nanocrystalline

Ni (a minimum of ~12 nm) [56]. Furthermore, the room temperature spontaneous growth of individual grains that has recently been observed in some nanocrystalline metals appears to be limited to specimens of high purity [57]. Each of these observations suggests that impurity atoms, even in relatively small quantities, play a crucial role in stabilizing the microstructure.

5. Conclusions

This paper provides direct experimental evidence of the segregation of impurity elements to grain boundaries in pure nanocrystalline metals. There is a strong correlation between the strength and ductility of nc-Al thin films and the amount of O segregation that was measured for each set of films. The increased strength (and reduced ductility) is beyond that which could be expected due to solid solution strengthening and is attributed to a change in the critical stress required for stress-assisted grain boundary migration and associated grain growth. The fact that dramatic changes in properties have now been directly associated with very small amounts of impurities offers the potential to tailor the properties of nanocrystalline alloys by local spatially controlled doping.

Acknowledgements

This work is supported by the Australian Research Council (ARC) and the National Science Foundation (NSF) Materials Network Program, grant number DMR-1008222. The authors are grateful for scientific and technical input and support from the Australian Microscopy & Microanalysis Research Facility (AMMRF) node at the University of Sydney and financial support from the AMMRF travel and access program. DG acknowledges additional support through start-up funding from the University of Pennsylvania. The authors are also grateful for stimulating discussions with T.J. Rupert and B. Gault.

References

[1] Meyers MA, Mishra A, Benson DJ. Prog Mater Sci 2006;51:427.
[2] Bai X-M, Voter AF, Hoagland RG, Nastasi M, Uberuaga BP. Science 2010;327:1631.
[3] Choi P, da Silva M, Klement U, Al-Kassab T, Kirchheim R. Acta Mater 2005;53:4473.
[4] Jin M, Minor AM, Morris Jr JW. Thin Solid Films 2007;515:3202.
[5] Jin M, Minor AM, Stach EA, Morris JW. Acta Mater 2004;52:5381.
[6] Zhang K, Weertman JR, Eastman JA. Appl Phys Lett 2005:87.
[7] Brandstetter S, Zhang K, Escuadro A, Weertman JR, Van Swygenhoven H. Scripta Mater 2008;58:61.
[8] Pan D, Kuwano S, Fujita T, Chen MW. Nano Lett 2007;7:2108.
[9] Fan GJ, Fu LF, Choo H, Liaw PK, Browning ND. Acta Mater 2006;54:4781.
[10] Gianola DS, Eberl C, Cheng X, Hemker KJ. Adv Mater 2008;20:303.
[11] Gianola DS, Van Petegem S, Legros M, Brandstetter S, Van Swygenhoven H, Hemker KJ. Acta Mater 2006;54:2253.
[12] Gianola DS, Warner DH, Molinari JF, Hemker KJ. Scripta Mater 2006;55:649.
[13] Meirom RA, Alsem DH, Romasco AL, Clark T, Polcawich RG, Pulskamp JS, et al. Acta Mater 2011;59:1141.
[14] Legros M, Gianola DS, Hemker KJ. Acta Mater 2008;56:3380.
[15] Gianola DS, Mendis BG, Cheng XM, Hemker KJ. Mater Sci Eng A 2008;483–84:637.
[16] Elsener A, Politano O, Derlet PM, Van Swygenhoven H. Acta Mater 2009;57:1988.
[17] Zhou F, Lee J, Dallek S, Lavernia EJ. J Mater Res 2001;16:3451.
[18] Liu F, Chen Z, Yang W, Yang CL, Wang HF, Yang GC. Mater Sci Eng A 2007;457:13.
[19] Kirchheim R. Acta Mater 2002;50:413.
[20] Felfer P, Ringer SP, Cairney JM. Ultramicroscopy 2011;111:435.
[21] Gianola DS, Hemker KJ, Legros M, Sharpe Jr WN. TMS Lett 2004:1.
[22] Gianola DS, Eberl C. JOM-J Miner Met Mater Soc 2009;61:24.
[23] Sharpe WN Jr, Pulskamp JS, Gianola DS, Mendis BG, Eberl C, Polcawich R, et al. In: Proceedings of the 2006 ASME annual meeting, Chicago, IL; 2006.
[24] Thompson K, Lawrence D, Larson DJ, Olson JD, Kelly TF, Gorman B. Ultramicroscopy 2007;107:131.
[25] Felfer P, Alam T, Ringer SP, Cairney JM. Microsc Res Tech 2011, doi:10.1002/jemt.21081. [Epub ahead of print].
[26] Gault B, de Geuser F, Stephenson LT, Moody MP, Muddle BC, Ringer SP. Microsc Microanal 2008;14:296.
[27] Krakauer BW, Seidman DN. Phys Rev B 1993;48:6724.
[28] Ina K, Koizumi H. Mater Sci Eng A 2004;387:390.
[29] Sigle W, Richter G, Ruehle M, Schmidt S. Appl Phys Lett 1999;89:121911.
[30] Ruan S, Torres KL, Thompson GB, Schuh CA. Ultramicroscopy 2011;111:1062.
[31] Seidman DN. Annu Rev Mater Res 2007;37:127.
[32] Blavette D, Duval P, Letellier L, Guttmann M. Acta Mater 1996;44:4995.
[33] Hellman OC, Vandenbroucke JA, Rusing J, Isheim D, Seidman DN. Microsc Microanal 2000;6:437.
[34] Haque MA, Saif MTA. Proc Natl Acad Sci USA 2004;101:6335.
[35] Fleichner RL. Solid solution hardening. In: Peckner D, editor. The strengthening of metals. New York: Reinhold; 1964. p. 93.
[36] Labusch R. Phys Stat Solid 1970;41:659.
[37] Courtney TH. Mechanical behavior of materials. Boston: McGraw-Hill; 1999.
[38] Rupert TJ CTJ, Schuh CA. Acta Mater 2011;59:1619.
[39] Gibbs JW. The collected works of J.W. Gibbs. New York City: Longmans, Green; 1928.
[40] McLean D. Grain boundaries in metals. Oxford: Clarendon; 1957.
[41] Weissmuller J. Nanostruct Mater 1993;3:261.
[42] Weissmuller J. J Mater Res 1994;9:4.
[43] Millett PC, Selvam RP, Saxena A. Acta Mater 2007;55:2329.
[44] Krill CE, Klein R, Janes S, Birringer R. In: Yavari AR, editor. Mechanically alloyed and nanocrystalline materials: ismanam-94, vol. 179; 1995. p. 443.
[45] Caro A, Van Swygenhoven H. Phys Rev B 2001:63.
[46] Cahn JW, Mishin Y, Suzuki A. Acta Mater 2006;54:4953.
[47] Rupert TJ, Gianola DS, Gan Y, Hemker KJ. Science 2009;326:1686.
[48] Kumar KS, Van Swygenhoven H, Suresh S. Acta Mater 2003;51:5743.
[49] Yamakov V, Wolf D, Phillpot SR, Mukherjee AK, Gleiter H. Nat Mater 2002;1:45.
[50] Van Swygenhoven H, Derlet PA. Phys Rev B 2001:64.
[51] Chen MW, Ma E, Hemker KJ, Sheng HW, Wang YM, Cheng XM. Science 2003;300:1275.
[52] Detor AJ, Schuh CA. J Mater Res 2007;22:3233.
[53] Dieter G. Mechanical metallurgy. New York: McGraw-Hill; 1986.
[54] Haque MA, Saif MTA. Scripta Mater 2002;47:863.
[55] Zhilyaev AP, Langdon TG. Prog Mater Sci 2008;53:893.
[56] Schuh CA, Nieh TG, Iwasaki H. Acta Mater 2003;51:431.
[57] Ames M, Markmann J, Karos R, Michels A, Tschoepe A, Birringer R. Acta Mater 2008;56:4255.